Engineering space-variant inhomogeneous media for polarization control

Uriel Levy, Chia-Ho Tsai, Lin Pang, and Yeshaiahu Fainman

Department of Electrical and Computer Engineering, University of California, San Diego, 9500 Gilman Drive,
La Jolla, California 92093-0407

Novel devices for converting a linear polarization state to radial or azimuthal polarization states are realized by use of space-variant inhomogeneous media on a subwavelength scale. The two designs presented use form birefringence to locally transform the polarization state. The devices are fabricated in a GaAs substrate for operation in the far-infrared wavelength range. The experimental characterization is in good agreement with the designs, demonstrating high conversion efficiency. © 2004 Optical Society of America

OCIS codes: 230.5440, 090.1970.

Subwavelength-scale periodic inhomogeneous structures have been engineered to artificially create unique anisotropic[1,2] and dispersive[3,4] characteristics. Furthermore, such structures designed in resonance[5,6] can implement photonic crystal lattices. Space-variant subwavelength structures were also introduced for the realization of polarization-selective elements.[7] Recently, it was shown that applications such as laser machining[8] can be significantly enhanced if a radial polarization source can be used. Radial polarization can also be used to achieve a reduced focal spot size of a focused laser beam.[9] Existing approaches for achieving such polarization characteristics use the interference of two linearly polarized laser beams[10] or a special liquid-crystal cell with space-variant twist angles.[11] However, the first approach suffers from low efficiency and difficulty of integration, and the second approach is based on an unconventional liquid-crystal cell fabrication. More recently, an approach based on subwavelength diffractive optical elements[12] was used to achieve radially and azimuthally polarized light. However, since this implementation used circularly polarized input light, an additional quarter-wave retardation plate must be introduced when operating with commonly used linearly polarized laser sources. Moreover, the period of the subwavelength structure[12] increases linearly with radial coordinate $\hat{r}$, resulting in a relatively large hole in the central portion of the element, which reduces the effective conversion area and the conversion efficiency.

In this Letter we introduce novel devices that convert a linear polarization state to radial and azimuthal polarization states. Our devices are realized by use of space-variant inhomogeneous media (SVIM) on a subwavelength scale. This realizes locally varying form birefringence and offers relatively high conversion efficiency. It is well known that subwavelength periodic structures can be used to engineer a polarization dispersion relation for propagating TE and TM polarized optical fields. If the depth of the periodic structure is designed to introduce a π phase shift between the TE and the TM components, the device acts as a half-wave retardation plate, rotating the polarization of the incident linearly polarized field. The rotation angle is twice the angle between the

polarization vector of the incident field and the optic axis of the form-birefringent element. By controlling the orientation of the form-birefringent structure, we can engineer the amount of rotation in a space-variant manner, thereby creating any desired polarization distribution within the aperture of the incident field.

Our basic design considers an incident field propagating in the z direction, linearly polarized along the x axis [P_i in Fig. 1(a)]. For our application we wish to construct a beam with a space-variant polarization state linearly polarized in the radial direction along the $\hat{r}$ axis in the polar coordinate system $(\hat{r}, \hat{\theta})$ [i.e., the polarization state of the output field P_o shown in Fig. 1(a) is oriented at an angle θ with respect to the x axis, as shown schematically in Fig. 1(b). Thus we need to create a half-wave retardation plate with its principal axis oriented at an angle $\theta/2$ with respect to the x-polarized input field. Grating vector $\mathbf{K}_g$ needed to achieve such a device must satisfy

$$\mathbf{K}_g = \frac{2\pi}{d(x,y)} \left(\cos\frac{\theta}{2}\,\hat{x} + \sin\frac{\theta}{2}\,\hat{y} \right)$$
$$= \frac{2\pi}{d(r,\theta)} \left(\cos\frac{\theta}{2}\,\hat{r} - \sin\frac{\theta}{2}\,\hat{\theta} \right), \qquad (1)$$

where $d(x, y)$ is the local period of the grating and angle θ is measured counterclockwise from the x axis. To achieve a continuous grating we must satisfy continuity condition $\nabla \times \mathbf{K}_g = 0$. Applying curl in polar coordinates and assuming a radial dependency of the grating period, i.e., $d(r, \theta) = d(r)$, we obtain

$$\mathbf{K}_g = \frac{2\pi}{a_0\sqrt{r}} \left(\cos\frac{\theta}{2}\,\hat{r} - \sin\frac{\theta}{2}\,\hat{\theta} \right), \qquad (2)$$
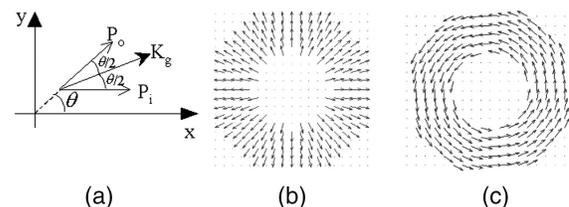

Fig. 1. Schematic diagram of the polarization transformation: (a) geometrical definitions, (b) radial polarization state, (c) azimuthal polarization state.

where a_0 is a constant chosen to meet fabrication constraints and aperture dimension requirements. It can be easily shown that for orthogonally polarized input (i.e., linear polarization along the y axis), the same element produces an azimuthal output polarization state, shown schematically in Fig. 1(c). It is evident from our design that the period of the SVIM is proportional to $\sqrt{r}$ and due to fabrication constraints resulting in a hole in its center [see Fig. 2(a)]. However, since with our approach the radius of the hole is smaller than that in Ref. 12 (with a period that increases linearly with r), we anticipate a significant increase in the conversion efficiency.

For the experimental realization we used a GaAs substrate that is transparent for operation at a wavelength of $\lambda = 10.6$ μm, supporting a CO_2 laser machining application. To avoid excessive line curvature requiring an ultrahigh-resolution mask, we restricted the minimal period to $d_{min} = 2$ μm. Furthermore, to avoid internal diffraction within the substrate, the maximum period should not exceed λ/n, where n is the refractive index of the substrate; thus $d_{max} = 3.05$ μm. By designing the outer radius to be 7 mm, we obtained $a_0 = 3.05/\sqrt{7}$ (μm$/\sqrt{mm}$) with corresponding inner radius $r_{min} = (d_{min}/a_0)^2 = 3$ mm. Thus the area not used because of the central hole is $\sim$18% of the total area. For comparison, using a previous design[12] with the same period restrictions, one obtains an $\sim$43% unused area, significantly reducing the conversion efficiency.

To further enhance the conversion efficiency, we explore a more effective density by assuming tangential dependency of the grating periodicity $d(r, \theta) = d(\theta)$ in Eq. (1), yielding

$$\mathbf{K}_g = \frac{2\pi}{d_0} \cos\left(\frac{\theta}{2}\right)\left[\cos\left(\frac{\theta}{2}\right)\hat{r} - \sin\left(\frac{\theta}{2}\right)\hat{\theta}\right], \qquad (3)$$

where d_0 is the period of the element along the horizontal axis ($\theta = 0$). The grating periodicity given by Eq. (3) is proportional to $[\cos(\theta/2)]^{-1}$ and increases toward infinity as $\theta \to \pi$ [see Fig. 2(b)]. Since the period should not exceed λ/n, only a limited angular portion of the element can be used. To overcome this issue, we chose the left-hand side of the element to mirror its right-hand side, as shown in Fig. 2(c). With such an arrangement the period size can be kept below the λ/n limit over the entire area of the device. This flipped geometry, however, causes the output polarization state along the left half-plane to be directed toward the center of the element rather than from the center outward. Although the near-field intensity pattern is not affected, the far-field pattern is different: Although for the first design a doughnut beam is obtained in the far field, this modified design produces a bright spot at the far-field origin. The latter issue can be easily overcome by incorporating a binary phase element with a π phase shift over the entire left half-plane relative to that of the entire right half-plane. For our design we set $d_0 = 2$ μm, leading to a maximal period size of $d_{max} = 2.82$ μm. As in the previous example, the outer dimension of the element is 7 mm.

Next we estimate the etching depth of the structure required to achieve the desired π phase

retardation by employing a rigorous coupled-wave analysis.[13] Although a rigorous coupled-wave analysis is valid for infinitely periodic structures, we used it as an approximation for our SVIM element because the period variation is slow on the wavelength scale. For a GaAs substrate with $n = 3.13$ (at $\lambda = 10.6$ μm) and a duty ratio of 50%, the required grating depth to achieve π phase retardation is 5.5 μm. This calculation assumes a rectangular groove shape; although such a profile is achievable, it gives rise to an undesired Fresnel reflection at the grating–air boundary. Furthermore, the reflection coefficient depends on the polarization ($\sim$5% for TM and $\sim$10% for TE polarization states), resulting in deviation from the desired output polarization state. To minimize reflection effects, we fabricated a trapezoidal component[1] with a duty ratio that gradually decreases from 65% to 25%. For this profile the desired depth is 6 μm, and the expected reflection reduced to 6% for TE and 5% for TM polarizations.

For fabrication of the designed devices, we employed a standard microfabrication procedure with electron-beam mask generation followed by photolithography and chemically assisted ion-beam etching. The mask pattern was transferred into the photoresist (BPRS100) by a high-resolution lithography process. The chemically assisted ion-beam etching process is used to transfer the pattern onto the GaAs substrate, which is antireflection coated on its backside to avoid surface reflection. Figure 3 shows a scanning electron microscope image of the device. Its profile closely matches the design requirements.

Characterization of the fabricated SVIM devices was performed with a plane wave derived from a single-mode, linearly polarized CO_2 laser source (Synrad 48-1). To translate the polarization rotation into an easily measurable amplitude modulation, a
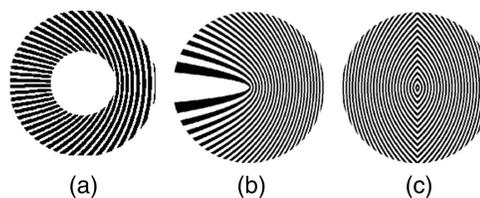

Fig. 2. Unscaled image of the designed polarization transformer elements: (a) element with period size varying along the radial axis, (b) element with period size varying along the tangential axis, (c) element constructed by using a symmetric version of the tangential design.
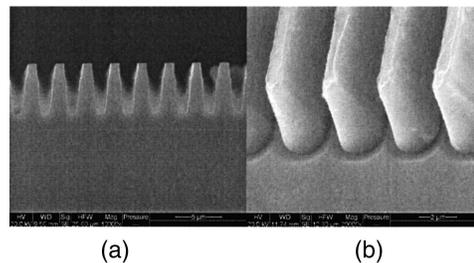

Fig. 3. Scanning electron microscope photograph of the fabricated polarization transformer element: (a) cross section, (b) enlarged side view.
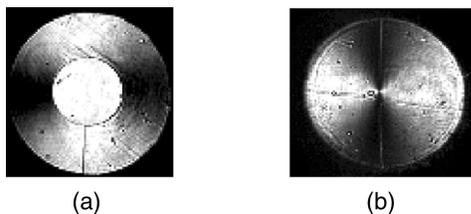
(a)   (b)

Fig. 4. Experimentally obtained image of the polarization transformer element illuminated by a linearly polarized beam. A cross polarizer is placed behind the element. (a) Design based on Fig. 2(a). The element was aligned with its horizontal axis parallel to the direction of the linearly polarized incident field. (b) Design based on Fig. 2(c). The element was aligned with its horizontal axis perpendicular to the direction of the linearly polarized incident field.
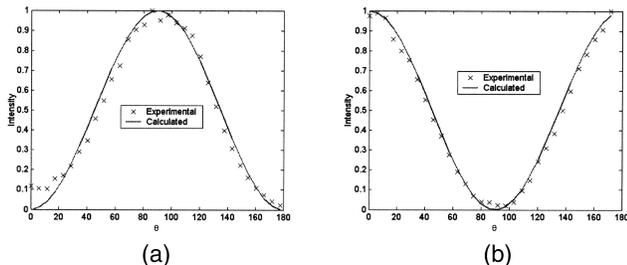

(a)   (b)

Fig. 5. Quantitative characterization of the designs presented in (a) Figs. 2(a) and (b) 2(c) by use of an angular cross section. The experimental data were obtained by digital integration across the radial coordinate of Figs. 4(a) and 4(b), respectively. The calculated curves were obtained with Eqs. (4) and (5).

linear polarizer was placed behind the element, and the resulting intensity-modulated image was detected with an Indigo IR camera (Omega, 160×128 pixels). The expected intensity profile is

$$I_r = E_{\text{out}} E_{\text{out}}^* = \sin^2(\theta), \qquad (4)$$

$$I_\theta = E_{\text{out}} E_{\text{out}}^* = \cos^2(\theta) \qquad (5)$$

for radial and azimuthal polarization conversion, respectively. The output field distribution is given by $E_{\text{out}} = PR(\theta)E_{\text{in}}$, with Jones matrix

$$P = \begin{bmatrix} 0 & 0 \\ 0 & 1 \end{bmatrix}$$

for the output polarizer;

$$R(\theta) = \begin{bmatrix} \cos\theta & \sin\theta \\ -\sin\theta & \cos\theta \end{bmatrix}$$

for the rotation matrix representing the SVIM element; and E_{in} being the incident beam linearly polarized along the x axis, $E_{\text{in}} = [1, 0]^T$, or along the y axis, $E_{\text{in}} = [0, 1]^T$, to achieve radial or azimuthal polarization, respectively. The element fabricated

with our first design [Fig. 2(a)] was aligned with its horizontal axis parallel to the incident polarization state, demonstrating a radially polarized beam. The field is transmitted through a crossed linear polarizer, producing the intensity distribution shown in Fig. 4(a). By integrating the measured data across the radial coordinate, we generate an angular-dependence curve, compared in Fig. 5(a) with the calculated curve [Eq. (4)]. The measured and calculated results are found in good agreement. Similarly, the second element [Fig. 2(c)] was aligned with its horizontal axis perpendicular to the incident polarization state to demonstrate the alternative, azimuthally polarized beam, producing the intensity distribution shown in Fig. 4(b). Figure 5(b) compares the measured and calculated angular dependence [Eq. (5)], demonstrating good agreement between the two curves.

We have presented novel devices for converting a linear polarization state into radial or azimuthal polarization states. The devices were realized by use of SVIM on a subwavelength scale, offering relatively high conversion efficiency. Two novel polarization conversion concepts were introduced. The basic design allows a gradual increase of the grating period along the radial coordinate to maintain the continuity of the grating; nevertheless, an annular element shape is required (although the central hole is significantly reduced compared with the previously reported approach). With the second design the central hole is eliminated by allowing the period size to vary along the tangential coordinate. On the basis of the above designs, SVIM elements were fabricated and used to demonstrate the polarization conversion functionality. The experimental results closely matched the theoretical expectations, proving the validity of the concepts.

U. Levy's e-mail address is ulevy@ece.ucsd.edu.

References

1. I. Richter, P. C. Sun, F. Xu, and Y. Fainman, Appl. Opt. **34,** 2421 (1995).
2. F. Xu, R. Tyan, P. C. Sun, C. Cheng, A. Scherer, and Y. Fainman, Opt. Lett. **20,** 2457 (1995).
3. C. Gu and P. Yeh, Opt. Lett. **21,** 504 (1996).
4. U. Levy and Y. Fainman, J. Opt. Soc. Am. A **21,** 881 (2004).
5. R. Tyan, P. C. Sun, A. Scherer, and Y. Fainman, Opt. Lett. **21,** 761 (1996).
6. R. Tyan, A. Salvekar, C. Cheng, A. Scherer, F. Xu, P. C. Sun, and Y. Fainman, J. Opt. Soc. Am. A **14,** 1627 (1997).
7. F. Xu, R. Tyan, P. C. Sun, Y. Fainman, C. Cheng, and A. Scherer, Opt. Lett. **21,** 1513 (1996).
8. A. V. Nesterov and V. G. Niziev, J. Phys. D **33,** 1817 (2000).
9. S. Quabis, R. Dorn, M. Eberler, O. Glockl, and G. Leuchs, Opt. Commun. **179,** 1 (2000).
10. S. C. Tidwell, D. H. Ford, and W. D. Kimura, Appl. Opt. **29,** 2234 (1990).
11. M. Stalder and M. Schadt, Opt. Lett. **21,** 1948 (1996).
12. Z. Bomzon, G. Biener, V. Kleiner, and E. Hasman, Opt. Lett. **27,** 285 (2002).
13. M. G. Moharam and T. K. Gaylord, J. Opt. Soc. Am. **72,** 1385 (1982).